ELSEVIER

PII: S0032-3861(97)00149-3

Polymer Vol. 38 No. 24, pp. 5953–5967, 1997

0032-3861/97/$17.00 + 0.00

Relationship between drawability of poly(vinyl alcohol) films prepared from semi-dilute solutions and phase separation of the solutions studied in terms of stereo-regularity and degree of polymerization

Masaru Matsuo*, Yuri Sugiura and Satomi Takematsu
Department of Textile and Apparel Science, Faculty of Human Life and Environment, Nara Women's University, Nara 630, Japan

and Tetsuya Ogita, Takashi Sakabe and Ryohei Nakamura
Department of Materials Science and Engineering, Faculty of Engineering, Yamagata University, Yonezawa 992, Japan
(Received 22 January 1997)

The phase separation of poly(vinyl alcohol) (PVA) in dimethyl sulfoxide/water mixtures was investigated by using light scattering techniques in terms of the degree of polymerization and stereo-regularity. Atactic (at-) and syndiotactic (st-) PVA, the degrees of polymerization (P) being 17900 and 1980, respectively, were used as test specimens. The analysis was mainly performed in comparison with previous results obtained for at-PVA ($P = 2000$) whose degree of polymerization is similar to that ($P = 1980$) of st-PVA, but lower than that ($P = 17900$) of at-PVA used in the present work. The phase separation occurred rapidly when the content of dimethyl sulfoxide in the mixed solvent was 50–70 vol%. This tendency was found to be significant for st-PVA with high stereo-regularity, but to be almost independent of the degree of polymerization of at-PVA. The logarithm of scattered intensity from at- and st-PVA solutions increased linearly with time in the initial stage of the phase separation. If this phenomenon could be analysed within the framework of the linear theory of spinodal decomposition proposed by Cahn (*J. Chem. Phys.*, 1965, **42**, 93) the phase diagram of st-PVA was classified into four regions: (I) a homogeneous sol region, (II) a sol region under spinodal temperature, indicating only spinodal decomposition, (III) a gel region under the spinodal curve, indicating simultaneous advance of both gelation and spinodal decomposition, and (IV) a gel region above the spinodal line, independent of liquid–liquid separation. On the other hand, for at-PVA, region II could not be observed and region IV existed only in a very narrow temperature range, which is similar to the result observed for at-PVA ($P = 2000$) solutions in previous work. The drawability of the dried gel film was affected by the composition of the solvent mixture and by quenching temperature of the solutions, but it was hardly affected by the stereo-regularity. This interesting phenomenon is discussed in terms of morphology of gels and films, as studied by crystallinity, X-ray diffraction, birefringence and small angle light scattering under Hv polarization condition. As the results show, it turned out that the greatest significant drawability is related to a continuous tissue with honeycomb-like structure associated with rapid phase separation of PVA solutions due to thermodynamic instability. © 1997 Elsevier Science Ltd.

(Keywords: phase separation; poly(vinyl alcohol); dimethyl sulfoxide)

INTRODUCTION

The production of high modulus and high strength poly(vinyl alcohol) (PVA) films and/or fibres has been extensively investigated and good results have been obtained by drawing of dried gel films prepared by crystallization from semi-dilute solutions in H_2O and dimethyl sulfoxide (Me_2SO) mixtures[1–10]. According to their reports, the drawability of PVA gel films was discussed in terms of the degree of polymerization (P), co-solvent composition (Me_2SO/H_2O by volume), concentration of solution and quenching temperature of solution. The co-solvent of Me_2SO and H_2O mixtures has one of the interesting characteristics that the solvent mixtures ranging from 50 to 70 vol% Me_2SO do not freeze at $-100°C$[11,12]. Through a series of experimental results, it was found that the co-solvent composition and the quenching temperature of the solutions prepared from the co-solvent cause a significant effect on the drawability of films obtained by drying the swollen gels prepared from the solution. Sawatari *et al.*[5] have reported that the dried gel films of atactic (at-) PVA with P of 2000 and 4400, prepared from the solution whose content of Me_2SO in the mixed solvent is 70 vol%, assure facile drawability and the films are more transparent than films prepared from solutions with other compositions. The transparency indicating a random array of crystallites that are much smaller

* To whom correspondence should be addressed

than the wavelength of an incident He–Ne gas laser beam was more pronounced at the gelation temperature[5]. Based on these results, they pointed out that the deformation mechanism of at-PVA dry gel films is quite different from ultradrawing of ultra-high molecular weight polyethylene (UHMWPE) films prepared by gelation/crystallization from dilute solutions. Namely, the UHMWPE film is composed of large crystal lamellae, and the drawing mechanism is associated with crystal transformation from a folded to a fibrous type[13–16]. In contrast, small angle X-ray scattering and unusual *H*v light scattering from drawn at-PVA films indicated that the preferential orientation of the *b*-axes (crystal chain axes) of PVA films is due to the rotation of crystallites around its own axes perpendicular to the chain axis rather than the crystal transformation[5].

In a previous paper[6], phase separation of at-PVA with $P = 2000$ in Me_2SO/H_2O mixtures was investigated by elastic scattering on the basis of the concept that the correlation between the transparency and facile drawability of PVA films is attributed to the relative rates of the phase separation associated with spinodal decomposition. Actually, a plot of the logarithm of the scattered intensity against time yielded a straight line in the initial stage of the phase separation and deviated from the linear relationship in the later stage. However, the peak position of the curve of the growth rate of concentration fluctuation against scattering vector shifted slightly towards the scattering centre with increasing difference between the measurable temperature and spinodal temperature defined by Cahn's theory[17,18]. This phenomenon could not be explained in terms of the concept of pure spinodal decomposition[17–21]. At the later stage, an X-type pattern could be observed under the *H*v polarization condition, indicating the existence of a rod-like texture, the optical axes being oriented parallel or perpendicular to the rod axis[22]. From this viewpoint, a question can arise as to whether or not the phase separation of PVA solutions is clearly attributed only to pure spinodal decomposition even in the time scale range assuring the linear relationship.

Another interesting question is why the greatest significant drawability could be realized by using dry gels prepared by immediately quenching solutions at $-50°C$[5]. Such rapid phase separation is obviously thought to be due to the independence of nuclear growth[6]. Incidentally, when the solutions stored for the period assuring the linear relationship was quenched at $-50°C$, drawability of the resulting dry gel films was somewhat lower than that of dry gels prepared without the storage period.

As one approach to the analysis of the two questions, this paper deals with the kinetics of the phase separation of at-PVA and syndiotactic (st-) PVA solutions prepared from a co-solvent of Me_2SO and H_2O as well as the morphology and mechanical properties of the resulting films. The *P* of at-PVA and st-PVA are 17900 and 1980, respectively. The results were compared with previous data for at-PVA ($P = 2000$) solutions.

EXPERIMENTAL

at-PVA ($P = 17900$) powder and st-PVA ($P = 1980$) powder were used. The degree of hydrolysis of the at-PVA was 98%, while that of st-PVA was 99.4% and the syndiotactic diad content was 61.2%. Mixtures of Me_2SO and H_2O were used as solvents for the at-PVA and st-PVA. When the content of Me_2SO in the mixed solvent was 70 vol%, the co-solvent formation was designated as having a 70/30 composition according to the previous papers[5,6]. As discussed in the previous paper[5], two different co-solvents with 70/30 and 50/50 composition were used in the present experiments. The solutions were prepared by heating the well-blended polymer/solvent mixture at 105°C for 40 min, and the solution was quenched in a water bath at a constant temperature. After standing for five days in the water bath at a constant temperature, the test-tube containing the solutions was tilted. When the meniscus deformed, but the specimen did not flow under its own weight, we judged that the solution had gelled. As described in the previous paper[6], the lowest temperature at which the onset of gelation occurred within five days was defined as the gelation temperature. Furthermore, the gelation time was determined at a fixed temperature based on the same judgement as described above. The time-dependence of scattered intensity and that of photon correlation measurements were performed by the elastic and inelastic light scattering technique using a He–Ne gas laser (DLS-700 produced by Ohtsuka Electric Co.). Both methods were explained in detail in the previous paper[6].

The elongation was carried out for the at- and st-PVA dry gel films prepared by quenching solutions at $-80°C$, in which the concentrations of the former and latter solutions were 1 and 10 g dl^{-1}, respectively. For abbreviation, the unit of g dl^{-1} is termed %. The strips were clamped into a manual stretching device in such a way that the length to be drawn was 26 mm. Draw ratios were determined in the usual way by measuring the displacement of ink marks placed 2 mm apart on the specimen prior to drawing. The at-PVA film was placed under nitrogen at 160°C and elongated manually to a draw ratio of $\lambda = 7$ as the first stage. Immediately after stretching, the stretcher with the sample was quenched to room temperature. Elongation to draw ratios beyond $\lambda = 7$ was performed at 180°C in the second stage. This is due to the fact that the suitable temperature to realize the facile drawability shifts to a higher value as the draw ratio increases. The specimens were somewhat yellowed by carbonization. As for the st-PVA specimens, the drawings at the first and second stages were done at 180 and 200°C, respectively.

The density of the films was measured by pycnometry in a medium of *p*-xylene and carbon tetrachloride. Before the measurements were made, the specimen was cut into fragments and vacuum-dried. The crystallinities of at- and st-PVA films were calculated, by using the intrinsic densities of crystalline and amorphous phases, to be 1.345 and 1.269, respectively[23] on the basis of the assumption that the intrinsic densities are constant, independent of elongation. The density measurements were carried out several times to check the reproducibility of the values, since the difference in density between crystalline and amorphus phases is not large.

The characteristics of the films were estimated by X-ray analysis and load elongation. These methods have already been described elsewhere[5].

RESULTS AND DISCUSSION

Morphology and mechanical properties of the at- and st-PVA films with different drawability

In the previous paper[6], phase separation of at-PVA

($P = 2000$) in solutions with different Me_2SO/H_2O compositions was investigated by elastic light scattering techniques. In the initial stage of the phase separation for both the solutions, a plot of the logarithm of scattered intensity against time exhibited a straight line described within the framework of a linearized spinodal decomposition. However, no definite scattering peak from either solution, characterizing the latter stage of spinodal decomposition, was observed as a function of the scattering vector. Accordingly, Matsuo *et al.*[6] have pointed out that the phase separation of the at-PVA ($P = 2000$) is quite different from pure spinodal decomposition of amorphous polymer solutions[19] and liquid–liquid phase separation of amorphous polymer blends[20,21], as have been reported generally. As another important conclusion, it was confirmed that the gradual progression of phase separation of at-PVA solutions prepared from Me_2SO/H_2O mixtures, the compositions being 50/50 and 70/30, hampered facile drawability of the resulting films. That is, when at-PVA solutions stored for a few hours at 20°C were quenched at −50°C and were vacuum-dried at the same temperature, the tensile strength and Young's modulus of the drawn films become slightly lower than those of drawn films which were prepared by immediately quenching the solutions with the same composition as −50°C and vacuum-dried at the same temperature.

Based on the preliminary results for at-PVA ($P = 2000$)[5], the molecular weight-dependence of drawability of at-PVA films was investigated using specimens with $P = 17\,900$ as a function of the Me_2SO/H_2O composition and the temperature of quenching solutions. The five kinds of compositions, 40/60, 50/50, 60/40, 70/30 and 80/20, were chosen as mixed co-solvents, and the quenching temperatures were set at −80, −40, −10 and 20°C. At the 90/10 and 20/80 compositions, the gelation did not occur at 20°C. The films prepared under the various conditions were stretched under nitrogen at 160°C up to the maximum draw ratio and cooled down to room temperature immediately, in order to seek the best condition assuring significant drawability without carbonization. This condition is different from such an elongation one described in the Experimental section where specimens were somewhat yellowed by carbonization. The drawn films were clearly transparent without carbonization. *Figure 1* shows each maximum draw ratio and the corresponding birefringence, Young's modulus and tensile strength obtained for the films prepared under the indicated conditions. The maximum draw ratio could be realized by the elongation of films prepared by quenching at-PVA solution with the 60/40 composition at −80°C. This suggests that the molecular orientation and mechanical properties are strongly affected by the facile drawability, and the greatest significant drawability can be realized by the control of two factors: the content of Me_2SO in the mixed solvent and quenching temperature of the solution. The same phenomenon was confirmed for at-PVA with $P = 2000$ in the previous paper[5].

To give generality to the above experimental results, similar experiments were tried for st-PVA. Unfortunately, the amount of st-PVA furnished was too small to carry out the experiments for films prepared from solutions with various Me_2SO contents. Thus, detailed measurements were mainly limited to st-PVA films prepared from solutions with three compositions: 70/30, 60/40 and 50/50. The greatest significant drawability could be realized for specimens prepared under the same condition as at-PVA.

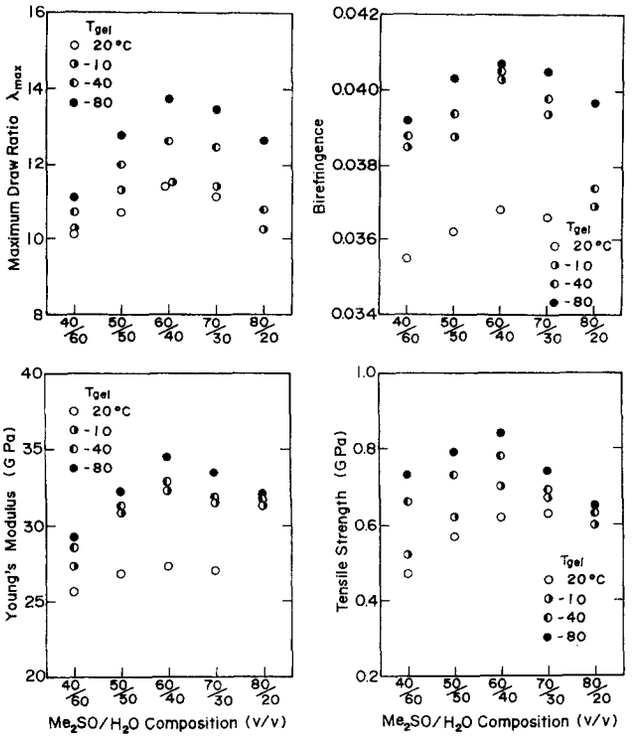

Figure 1 Maximum draw ratio, the corresponding birefringence, Young's modulus and tensile strength for drawn films prepared by the indicated compositions of Me_2SO/H_2O

Figure 2 shows the change in appearance of at- and st-PVA films prepared by quenching solutions with the 70/30 composition at the indicated temperatures, under scanning electron microscopy (SEM). The fibrillar texture shows honeycomb-like structure, the size of the holes becoming smaller as the quenching temperature decreases. The same tendency was observed for the 40/60, 50/50 and 60/40 compositions. In spite of the drastic changes of fibrous structure, the crystallinities of at- and st-PVA films slightly decreased from 20.4 to 19.8% and from 22 to 21.4%, respectively, as the quenching temperature was lowered from 20 to −80°C. Incidentally, it was confirmed that hole size for the 60/40 and 70/30 compositions were smaller than those for other compositions at gelation/crystallization temperatures < -10°C. This indicates that the dense network structure plays an important role in assuring high drawability, since inner stress within the film is transmitted smoothly in the stretching direction.

Figure 3 shows the time-dependence of light transmission of gels prepared from 1% at-PVA solution by gelation/crystallization at the indicated temperatures and stored at 20°C, in which the (a), (b) and (c) parts correspond to 50/50, 60/40 and 70/30 compositions, respectively. The decrease in transmission became more pronounced as the gelation/crystallization temperature increased. In particular, for 50/50 and 60/40 compositions, the drastic decrease at storage times < 3 h was observed for the gels prepared at 20°C and consequently the gels whitened. Furthermore, when solutions were quenched at 20°C and the resulting gels were stored for more than 8 h at 20°C, *Hv* light scattering patterns could be observed. The patterns were of X-type, indicating the existence of rod-like textures, the optical axes being oriented parallel or perpendicular to the rod

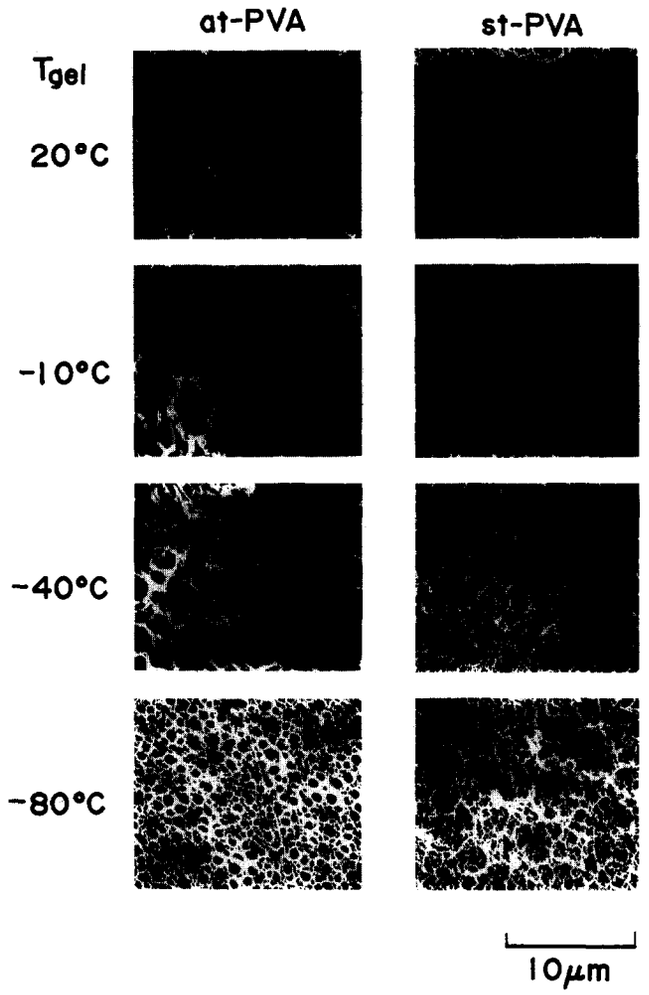

Figure 2 Scanning electron micrographs of at- and st-PVA films prepared by quenching solutions with the 70/30 composition at the indicated temperatures

axis. For the 70/30 composition, the transmission of the scattered beam through the gels, which were prepared at 20°C and maintained at the same temperature, became most intense among all the gels. However, the transmission gradually decreased with time, and a very small X-type pattern appeared after 20 h. This implies that the morphology of the gels is sensitive to gelation/crystallization temperature. In particular, for the gels prepared by quenching at −10 and −40°C, the morphology seems to be preserved during storage at room temperature. No *Hv* scattering pattern from the gels appeared. Also, the scattering pattern could not be observed for dried gel films. The same tendency was also confirmed for the gels prepared at −80°C. Thus, it was found that at-PVA fibrous tissue showing honeycomb-like structure in *Figure 2* does not exhibit any optical anisotropy.

Based on the results in *Figures 1–3*, we shall briefly refer to the morphology of gels and resulting films. For the gels prepared at 20°C, the scattering could not be observed at gelation times <3 h. However, the X-type pattern appeared gradually after the gelation time. In this process, a very weak broad overlapped X-ray diffraction from (101) and (10$\bar{1}$) planes also could be observed, which is not shown in this paper. Accordingly, it is evident that anisotropic rods were preformed with the further gradual development of gelation/crystallization accompanying molecular alignment in the polymer rich

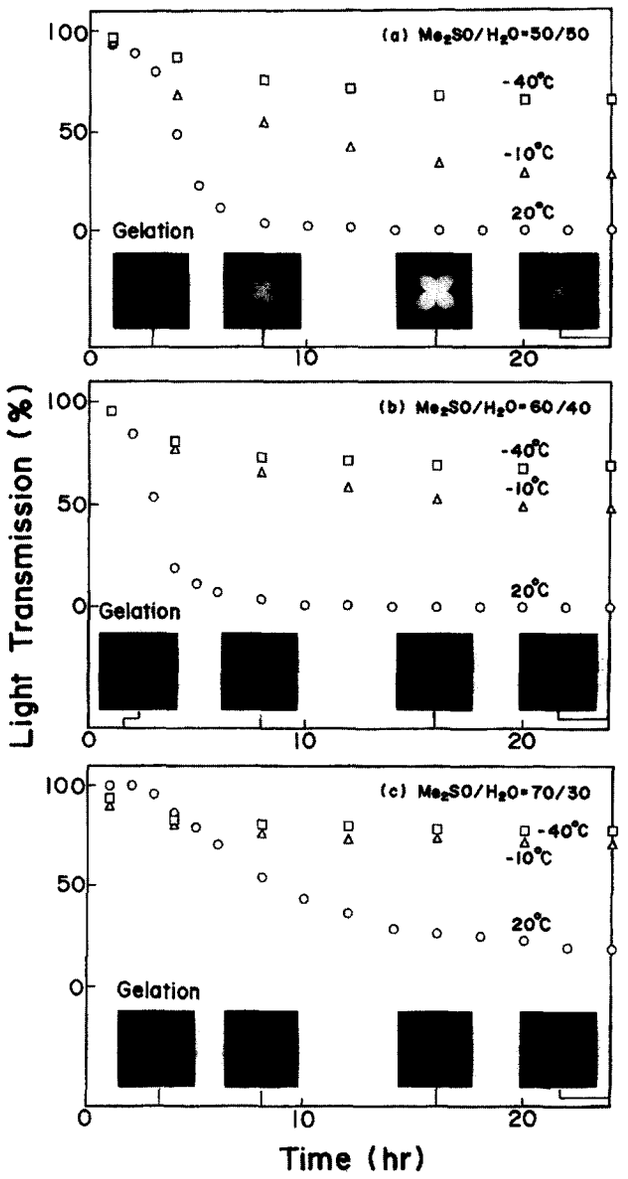

Figure 3 Time-dependence of light transmittance of gels by quenching 1% at-PVA solutions at the indicated temperatures, in which (a), (b) and (c) correspond to 50/50, 60/40 and 70/30 compositions, respectively. All patterns were observed at room temperature

phase. In contrast, when the gels were prepared by quenching solutions at lower temperatures (<10°C), immobilization of PVA chains by rapid gelation/crystallization did not allow the formation of ordered structure with optical anisotropy, but provided a random array of crystallites whose size was much smaller than the wavelength of an incident He–Ne gas laser beam.

Phase separation of the at- and st-PVA solutions by elastic light scattering

Apart from the instantaneous gelation at −10 and −40°C, it is of interest to consider the advance of gradual phase separation of the solutions at 20°C in relation to the appearance of anisotropic rods. Accordingly, the time-dependence of scattered intensity was measured during the isothermal phase separation process of the solutions at various scattering angles. *Figures 4* and *5* show the change in the logarithm plots of the scattered intensity against time at various q observed for 1% at- and st-PVA solutions with 70/30 composition, where the magnitude of the scattering vector, q, is given by

$q = (4\pi n/\lambda)\sin(\theta/2)$, λ, θ, and n being the wavelength of light in solution, the scattering angle and the refractive index of the solvent, respectively. The refractive index n was carefully measured by an Atago-2T (indexmeter produced by Alago Co.). The logarithm of the scattered intensity increased linearly with time in the initial stage of phase separation, indicating the possibility of successful analysis of the linear theory of spinodal decomposition proposed by Cahn[17]. With time, the logarithm of scattered intensity tends to deviate from the linear relationship, as has been observed for the later stage of spinodal decomposition of amorphous polymer blends[20,21]. The deviation shifts to shorter time scale as the temperature increases. This tendency was the same for both at- and st-PVA solutions. Comparing the behaviour in *Figures 4* and *5* with the previous results for at-PVA ($P = 2000$) (see Figure 1 of ref. 6), it turns out that the time scale of the deviation is almost independent of molecular weight and only depends on the stereo-regularity. That is, the deviation for the at-PVA ($P = 2000$) occurred at the same time scale for the at-PVA ($P = 17900$), but occurred at a time scale longer than for the st-PVA ($P = 1980$).

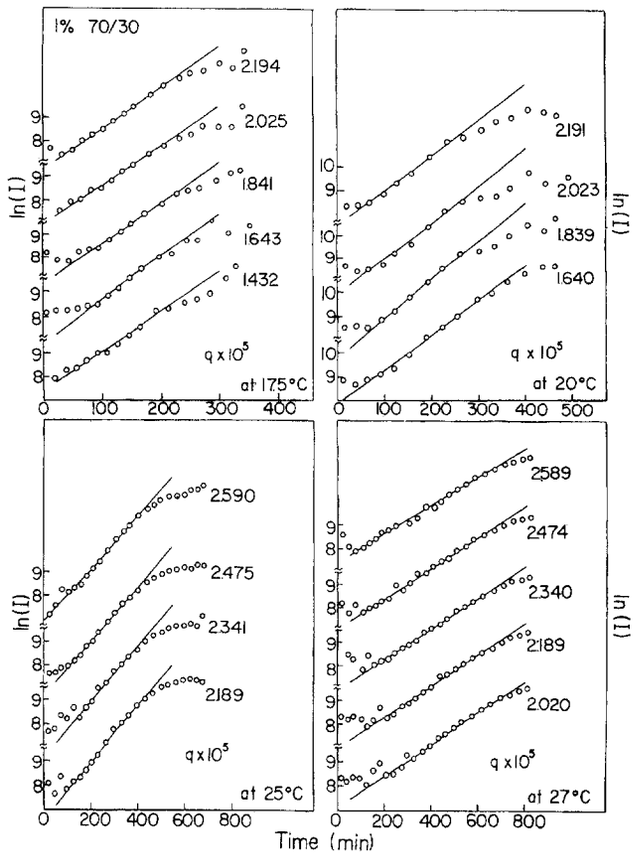

Figure 4 Change of the log scattered intensity against time at various q values measured for 1% at-PVA solutions with the 70/30 composition at various temperatures

If the linear relationship reflects the initial stage of spinodal decomposition as pointed out by Cahn[17], it is well known that the change in elastic scattered intensity in *Figures 4* and *5* can be given by[6]

$$I(q,t) = I(q,t=0)\exp[2R(q)t] \qquad (1)$$

where $I(q,t)$ is the scattered intensity at the time, t, after initiation of the spinodal decomposition, and $R(q)$ is the growth rate of concentration fluctuation given as a function of q; $R(q)$ is given by

$$R(q) = -D_c q^2\left\{\frac{\partial^2 f}{\partial c^2} + 2\kappa q^2\right\} \qquad (2)$$

where D_c is the translational diffusion coefficient of the molecules in solution, f is the free energy of mixing, c is the concentration of solution, and κ is the concentration-gradient energy coefficient defined by Cahn and Hilliard[18]. A linear relationship in the plot of $\ln(I)$ *versus* t at fixed q was also obtained for at- and st-PVA solutions with other concentrations at various temperatures.

Through a series of experimental results concerning the phase separation of at- and st-PVA solutions, a question can arise as to whether or not phase separation of PVA solutions is always attributed to the spinodal decomposition, if the linear relationship depicted in *Figures 4* and *5* can be observed. To pursue the detailed discussion, first the spinodal temperature, T_s, was estimated for at-PVA ($P = 17900$) and st-PVA

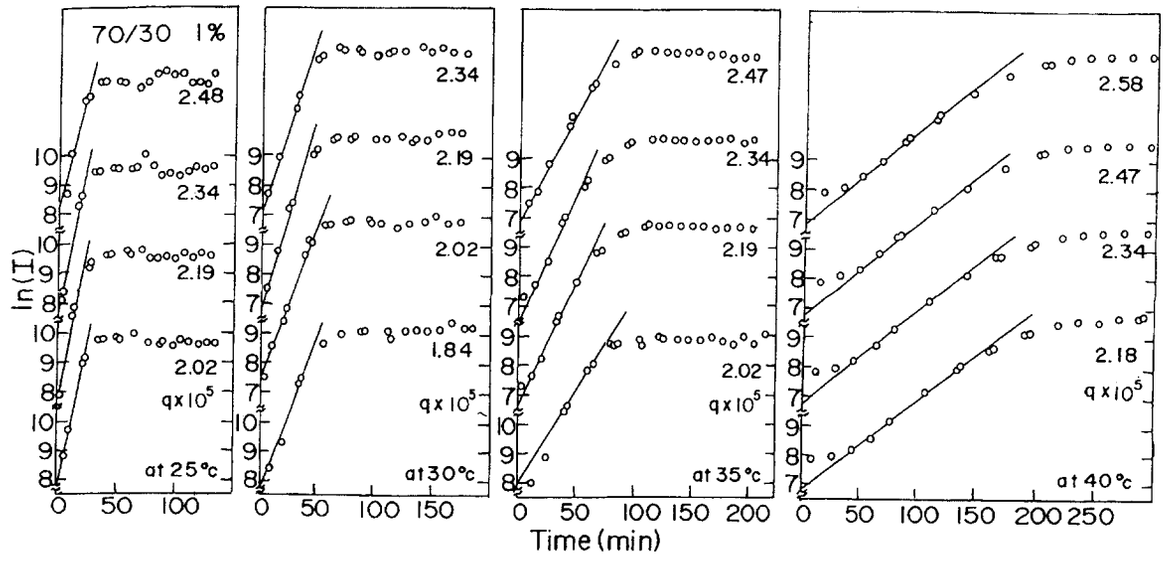

Figure 5 Change of the log scattered intensity against time at various q values measured for the 1% st-PVA solutions with the 70/30 composition at various temperatures

($P = 1980$) according to the linear Cahn's theory[17]. The treatment was described in the previous paper in detail[6]. *Table 1* shows the results. The previous data for the at-PVA ($P = 2000$) are included in this table. Incidentally, the values of $D_{app}(= D_c(\partial^2 f/\partial c^2))$, listed in *Table 2*, are efficiently estimated by obtaining an intercept at $q^2 = 0$ in the plot $R(q)/q^2$ *versus* q^2 by assuming pure spinodal decomposition. Because of the positive values of D_c by definition, the values of D_{app} take negative values characterizing unstable regions, leading to spinodal decomposition. The small values of $\partial^2 R(q)/\partial q^2|_{q=q_m}$, hence $D_{app}(\partial^2 R(q)/\partial q^2|_{q=q_m} = 8D_{app})$, indicate no appearance of a scattering maximum of intensity at the initial stage of spinodal decomposition. To observe a distinct scattering maximum in the linear spinodal decomposition regime, it is evident that the value of D_{app} must be usually two to three orders of magnitude greater. Here, it is seen that the spinodal temperature, T_s, listed in *Table 1*, shifts to higher value as the concentration of solution increases. This tendency is more pronounced for the 50/50 composition. This indicates that the phase separation of the 50/50 composition is more significant than that of the 70/30 composition when both solutions have the same concentration. The spinodal temperature, T_s, of the at-PVA solutions shifted to higher value with increasing molecular weight, when the co-solvent with the same composition

Table 1 Spinodal temperatures of several kinds of PVA solutions prepared with 70/30 and 50/50 compositions (°C)

		Concentrations ($g\,dl^{-1}$)						
Me_2SO/H_2O	PVA specimens	0.5	1	1.2	2	3	5	10
70/30	st-PVA ($P = 1980$)	38.3	41.9	—	45.0	47.8	—	—
	at-PVA ($P = 2000$)	—	20.7	—	—	—	30.3	34.6
	at-PVA ($P = 17900$)	25.5	30.5	33.2	—	—	—	—
50/50	st-PVA ($P = 1980$)	55.1	59.1	—	65.5	—	—	—
	at-PVA ($P = 2000$)	—	23.4	—	—	—	31.2	36.8
	at-PVA ($P = 17900$)	36.7	40.7	41.2	—	—	—	—

Table 2 Values of D_{app} for at- and st-PVA solutions (units: $-D_{app} \times 10^{-13} cm^2 s^{-1}$)

Temperature (°C)	at-PVA with 70/30 composition			at-PVA with 50/50 composition		
	0.5%	1.0%	1.2%	0.5%	1.0%	1.2%
12.5	1.18					
15.0	0.826					
17.5		1.04				
20.0	0.493	0.768	0.875			
22.0	0.298			1.80		
25.0		0.397	0.510	1.46		
27.0		0.219	0.352		1.50	2.20
30.0				0.835	1.02	1.90
32.5				0.459		
35.0					0.534	0.889
38.0					0.366	
38.5						0.411
	0.5%	1.0%	2.0%	0.5%	1.0%	2.0%
25.0	5.23	4.29				
28.0	2.94					
30.0	2.11	2.50				
33.0	1.53					
35.0		1.45	2.90			
38.0			2.22			
40.0		0.512	1.75			
43.0			1.03	4.41		
45.0				3.09	5.56	
48.0				2.51	4.13	
50.0				1.65	3.10	
53.0					1.85	3.26
58.0						2.10
60.0						1.47

was chosen. Furthermore, it is seen that the T_s value of the st-PVA with $P = 1980$ was higher than those of the at-PVA with $P = 17900$ and 2000. Such an interesting phenomenon is due to the fact that the stereo-regularity causes much more significant effect on the progression of phase separation rather than an increase in the degree of polymerization. The crystallinity of the resulting st-PVA films was slightly higher than that of the at-PVA films.

Figures 6a and *6b* show the concentration dependence of spinodal temperature (T_s) and gelation temperature for the st-PVA with 70/30 and 50/50 compositions, respectively, in which the dashed and solid curves correspond to spinodal and gelation temperatures, respectively. The dashed (spinodal) curve was drawn to follow the plotted point of T_s, while the solid (gelation) curve was drawn to follow a number of data for gelation temperature. At temperatures above the solid curve, the sol–gel transition cannot occur, while at temperatures below the solid curve, the gelation rate becomes faster as the temperature decreases. As can be seen in *Figure 6*, the phase diagram can be classified into four regions: (I) a homogeneous sol region, (II) a sol region under the spinodal temperature, indicating only spinodal decomposition, (III) a gel region under the spinodal curve, indicating simultaneous advance of both gelation and spinodal decomposition, and (IV) a gel region above the spinodal temperature, independent of liquid–liquid separation. This diagram is similar to the result by Komatsu *et al.* for aqueous PVA solutions[24], but is different from the previous results observed for at-PVA ($P = 2000$) in a Me_2SO/water mixture as co-solvent[6].

Figure 7 shows the phase diagram for at-PVA ($P = 17900$). It is seen that the spinodal points and sol–gel transition curves divided the phase diagram into three regions. Namely, region II, indicating only spinodal decomposition, could not be observed. Such a phase diagram is essentially the same as that for at-PVA ($P = 2000$), discussed in the previous paper[6].

Considering the series of experimental results in *Figures 4–7*, in addition to the previous results for at-PVA ($P = 2000$)[6], it may be expected that the dynamics of the sol–gel transition of PVA solutions is strongly affected by the stereo-regularity rather than by molecular weight. To check this, more detailed information on the gelation and spinodal decomposition must be obtained in terms of the morphological aspects. Accordingly, light scattered patterns under Hv polarization condition were observed as a function of temperature. The logarithmic plots of scattered intensity at $\theta = 90°$ as a function of time are presented as a reference. *Figure 8* shows the results for the 1% st-PVA solutions with 70/30 composition at 40°C and with 50/50 composition at 55°C, while *Figure 9* shows the results for the 1% at-PVA solutions with 70/30 composition at 20°C and with 50/50 composition at 27°C. For the st-PVA solution with 50/50 composition, 40°C is the temperature associated with the simultaneous advance of both gelation and spinodal decomposition, and 55°C for the 50/30 composition, associated with spinodal decomposition only, as shown in *Figures 6* and *7*. In the former case, Hv light scattering showed an indistinct circular type, indicating the formation of random array crystallites smaller than the wavelength of the incident beam, in the time scale showing the straight line of $\ln(I)$ *versus* time (t). In the latter case, the scattering showed an X-type pattern, indicating the formation of anisotropic rods composed of crystallites in the time scale showing the straight line of $\ln(I)$ *versus* t. The existence of crystallites was confirmed by X-ray diffraction measurements, in which the sample preparation was carried out according to the same

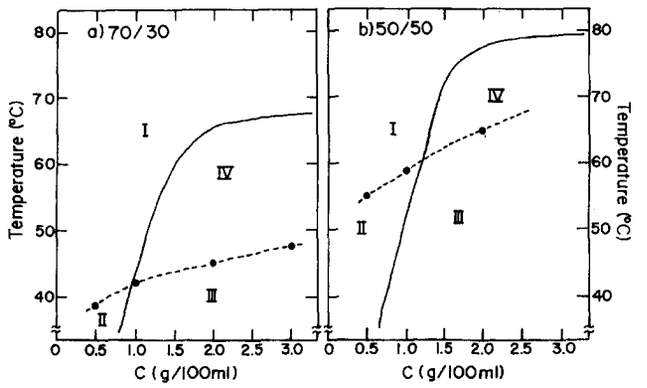

Figure 6 Spinodal and gelation temperatures *versus* concentration for st-PVA solutions: (a) 70/30 composition; (b) 50/50 composition. Solid curves show the gelation temperature *versus* concentration, and dashed curves show the spinodal line

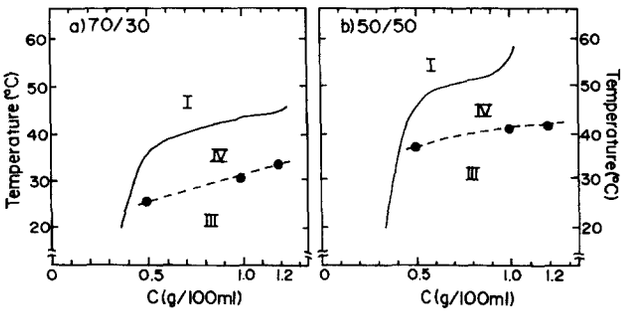

Figure 7 Spinodal and gelation temperatures *versus* concentration for at-PVA solutions: (a) 70/30 composition; (b) 50/50 composition. Solid curves show the gelation temperature *versus* concentration, and dashed curves show the spinodal line

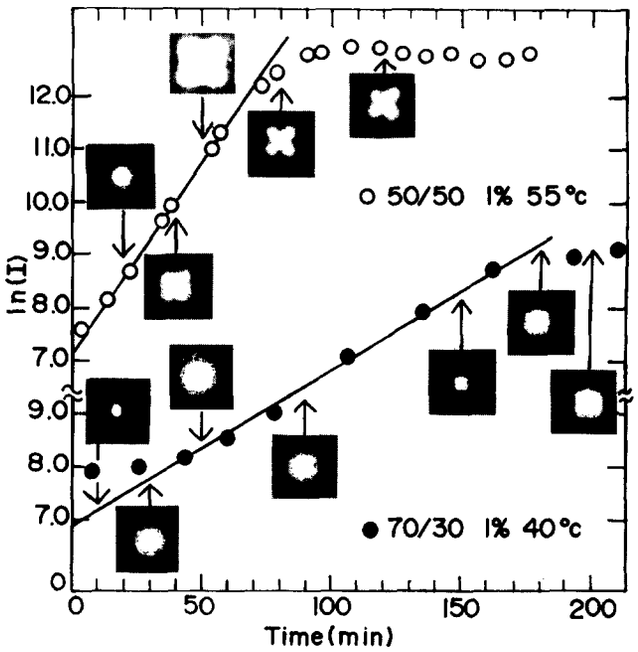

Figure 8 Change of $\ln(I)$ at $\theta = 90°$ and Hv light scattering patterns with time measured for the 1% st-PVA solutions with 70/30 composition at 40°C and 50/50 composition at 55°C

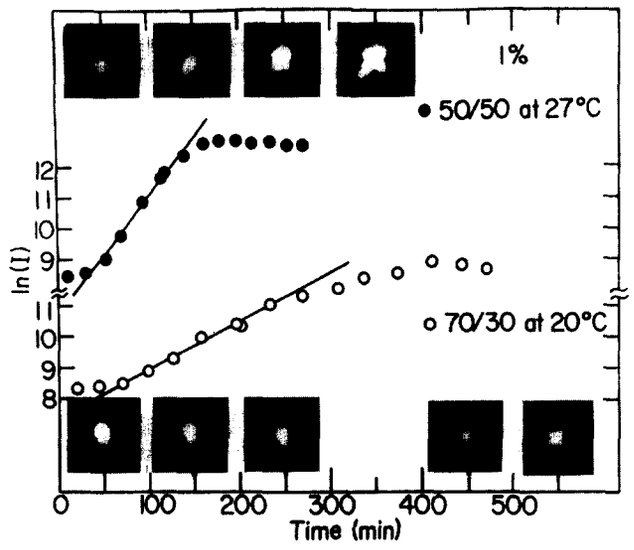

Figure 9 Change of $\ln(I)$ at $\theta = 90°C$ and Hv light scattering patterns with time measured for the 1% at-PVA solutions with 70/30 composition at 20°C and 50/50 composition at 27°C

process as the measurements in *Figures 8* and *9*. A weak broad overlapped intensity distribution from the (101) and (10$\bar{1}$) planes was observed during the periods of about 10–50 min for the 50/50 composition and about 90–130 min for the 70/30 composition, corresponding to each end of the linear portion of $\ln(I)$ *versus t*. For the at-PVA system, Hv light scattering patterns cannot be observed except as indistinct small spots, which is an artefact due to reflection of the incident beam in the time scale showing a straight line in the plot of $\ln(I)$ *versus t*. Even so, a very weak broad overlapped X-ray diffraction intensity distribution from the (101) and (10$\bar{1}$) planes was observed during the periods of about 80–120 min for the 50/50 composition and about 180–220 min for the 70/30 composition, corresponding to each end of the linear portion of $\ln(I)$ *versus t*. This tendency is almost the same as the previous results for at-PVA ($P = 2000$)[6].

With increasing time, the plot of $\ln(I)$ *versus t* deviates from the straight line and the corresponding X-type light scattering pattern becomes more distinct. As discussed before, the formation of rods with optical anisotropy is probably associated with the gradual development of gelation/crystallization in the polymer-rich phase. Thus, the deviation from the straight line in the $\ln(I)$ *versus t* plot is quite different from the concept of the later stage of spinodal decomposition of amorphous polymer blends[25]. That is, the further growth of concentration fluctuations associated with uphill diffusion for polymer blends is significant in the later stage of the spinodal decomposition and finally the concentration profile becomes similar to that of nucleation growth. Such a further growth of concentration fluctuation, however, is suppressed for PVA solutions because of immobilization of the PVA chains associated with crystallization.

As can be seen in *Figures 8* and *9*, the plot of $\ln(I)$ *versus t* for the 50/50 composition of st-PVA solution at 55°C deviates from linearity after 70 min, while it is linear up to 120 min for the same composition of at-PVA solution measured at 27°C. This means that 60 min corresponds to the final period of the initial stage, assuring a straight line of $\ln(I)$ *versus t* for the st-PVA solution at 55°C. On the other hand, 60 min for the at-PVA solution still corresponds to the initial stage of the quasi-spinodal decomposition at 27°C, although 27°C is lower than the measurable temperature (55°C) for the st-PVA solution. The same tendency could be observed for the 70/30 composition. These phenomena suggest that the progression of the phase separation of st-PVA solutions is faster than that of at-PVA ones.

As discussed before, the appearance of an X-type light scattering pattern and the weak broad overlapped X-ray diffraction from the (101) and (10$\bar{1}$) planes were observed during the process of phase separation of st-PVA solutions for the 50/50 composition at 55°C. Here, it should be noted that, if the phase diagrams in *Figure 6* are correct, the phase separation at region II of the st-PVA solution at 55°C must be dependent upon only the progression of the spinodal decomposition. However, the Hv light scattering showing an X-type pattern and the weak, broad X-ray diffraction indicated the existence of anisotropic rods in the solutions. This is in contradiction with the general concept of the initial stage of spinodal decomposition. To check the origin, the growth rate of concentration fluctuation $R(q)$ is plotted against q instead of $R(q)/q^2$ *versus* q^2 for obtaining the spinodal temperature T_s listed in *Table 1*. *Figures 10* and *11* showed the results for the st- and at-PVA solutions. The maximum growth rate $R(q_m)$ of concentration fluctuation increases with decreasing measurable temperature. The value of the scattering vector, q_m, shifts slightly towards the scattering centre with increasing difference $(T_s - T)$ between the measurable temperature, T, and spinodal temperature T_s. This tendency has already been confirmed for at-PVA ($P = 2000$)[6]. These phenomena are quite different from the principle of spinodal decomposition for amorphous polymer solutions proposed by van Aartsen[19]. According to his theory, the value of q_m increases with increasing difference $(T_s - T)$, if the range of molecular interaction associated with the mean square radius of gyration based on the concept of Debye and Woermann[26] is independent of temperature. Thus, the shift of $R(q_m)$ to a lower value of q on increasing the difference $(T_s - T)$ justified the earlier conclusion that neither the linearized theory of the spinodal decomposition proposed by van Aartsen[19] nor the theory of Cahn[17] is applicable for at-PVA ($P = 17900$) and st-PVA ($P = 1980$) solutions, since the phase separations for the st-PVA solutions with 1 and 2% concentrations are attributed to the advance of spinodal decomposition and gelation, as shown in the phase diagrams in *Figures 6* and *7*. For the 0.5% st-PVA solutions whose phase separation is thought from the phase diagram, to be due to pure spinodal decomposition the shift of $R(q_m)$ towards the scattering centre is in contradiction to the theory of van Aartsen[19]. This contradiction is probably due to the definition of gelation in the Experimental section, which cannot be applicable to the dilute solutions. Actually, at the macroscopic level, we could observe the gels locally in the 0.5% solutions at temperatures lower than T_s defined by the phase diagram in *Figure 6*, indicating the simultaneous advance of gelation and spinodal decomposition. Of course, it was impossible to observe a definite light scattering peak as a function of q characterizing the later stage of spinodal decomposition under depolarization and V_v polarization conditions[27]. Following Cahn's theory[17], the concentration fluctuation relating to equation (1) at the proper long

time t can be rewritten approximately as follows:

$$\langle |C(q,t) - C_0|^2 \rangle \sim \langle |C(q_m,t) - C_0|^2 \rangle \propto \exp[2R(q_m)t] \quad (3)$$

where $|C(q,t) - C_0|$ is the concentration fluctuation at t. Equation (3) suggests the existence of a scattering peak at θ_m from the relationship $q_m = (4\pi n/\lambda)\sin(\theta_m/2)$. Actually, the scattering peak has been observed at a later stage of spinodal decomposition for amorphous blend films[20,21]. No appearance of the scattering peak at the later stage of phase separation of PVA solutions is thought to be due to the very broad curve of $R(q)$ against q. In this case, a clear scattering peak cannot be observed at θ_m. Accordingly, a question can arise as to whether or not equation (2) associated with the linear Cahn's theory is applicable for the analysis of the linear relationship of $\ln(I)$ *versus* t in *Figures 4* and *5*. If the linear relationship does not follow the linear Cahn theory[17], equation (1) must be rewritten as follows:

$$I(q,t) = I(q,t=0)\exp[Q'(q,t)] \quad (4)$$

To satisfy the linear relationship of $\ln(I)$ *versus* t, $Q'(q,t)$ must be described as $Q(q,t)$, indicating variable separation of q and t. In this case, however, $Q(q)$ is not equivalent to $2R(q)$ and another theoretical representation must be proposed. Presumably, simultaneous advance of gelation/crystallization and spinodal decomposition must be taken into consideration.

Returning to *Figure 2*, close observation reveals that the size of holes of the honeycomb-like structure within the dry gel films becomes smaller with decreasing gelation/crystallization temperature, but the size within each specimen is almost constant. Such honeycomb-like structure is thought to be related to continuous tissue, characterizing spinodal decomposition. Although the size at −80°C was obviously within the limits of the characteristic wavelength for the polymer–solvent system, which can be estimated by using the distance of molecular interaction 30–300 Å[28], any scattering ring, however, could not be observed under depolarization V_v polarization conditions in spite of careful cover of the incident beam. If the honeycomb-like structure was already preformed in a swollen state, the spinodal

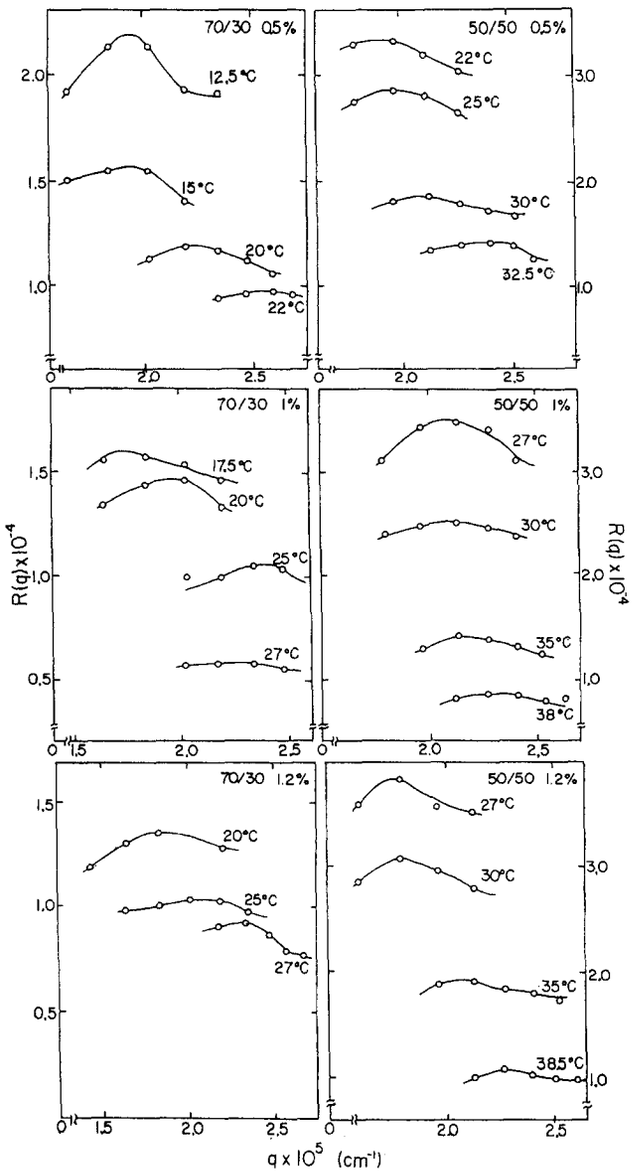

Figure 10 Variations of growth $R(q)$ of spinodal decomposition with q measured for the 1% at-PVA solutions

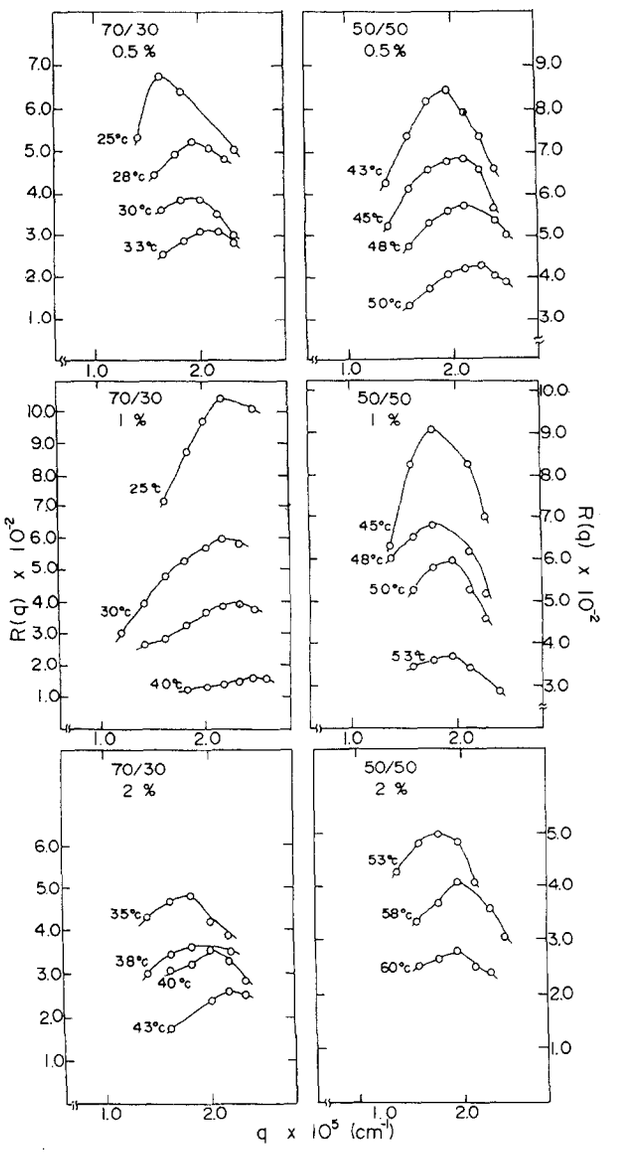

Figure 11 Variations of growth $R(q)$ of spinodal decomposition with q measured for the 1% st-PVA solutions

ring must be observed for swollen at-PVA gels. However, any scattering ring could not be observed. This essential fact remains an unresolved problem, as discussed before. In spite of the non-appearance of a spinodal ring, however, the honeycomb-like structure implies spinodal decomposition associated with rapid phase separation at temperatures $< -40°C$. If the phase separation was related to nucleation growth, it may be expected that such rapid phase separation could not be realized.

Based on a series of experimental results, it is evident that the phase separation is quite different from the concept of pure gelation associated with formation of a homogeneous infinite network from interpenetrating coils in the original solution. As pointed out by Labudzinska and Ziabicki[29], the gelation of PVA solutions is thought to be due to retarded phase separation. Namely, PVA solutions observed at elevated temperature are thermodynamically unstable at the gelation temperature and tend to incur phase separation. In such supercooled solutions, compact molecular aggregates may be formed and these connect to the heterogeneous network system (polymer-rich phase). It is likely that appearance of the continuous polymer-rich phase, indicating spinodal decomposition, causes the development of gelation/crystallization. A similar phenomenon was also confirmed by Wellinghoff *et al.*[30] for atactic polystyrene in carbon disulfide. This indicates that gelation can be realized by the extreme immobilization of polymer chains without cross-linking joints. Of course, by immobilization of PVA chains in the polymer-rich phase, some hydoxyl groups form hydrogen bonds as in the polymer-rich phase, i.e. gels, and so a cross-linked structure is formed. An increase in the amount of cross-linked structure by hydrogen bonding promotes gelation/crystallization. This phenomenon was confirmed by high-resolution solid-state ^{13}C nuclear magnetic resonance spectroscopy[31].

Considering the theoretical background for an inhomogeneous binary mixture composed of small molecules at the incompressible limit, the diffusion equation may be given approximately as[18]

$$\frac{\partial c}{\partial t} = D_c\left(\frac{\partial^2 f}{\partial c^2}\right)\nabla^2 c - 2D_c\kappa\nabla^4 c \qquad (5)$$

When the second term on the right-hand side in equation (5) is neglected, equation (5) reduces to a diffusion equation satisfying the second law of Fick, in which $D_c(\partial^2 f/\partial c^2)$ is the diffusion coefficient. In a spinodal decomposition system, $D_c(\partial^2 f/\partial c^2)$, corresponding to apparent diffusivity D_{app}, takes a negative value as listed in *Table 2*. At the later stage of spinodal decomposition, however, $D_c(\partial^2 f/\partial c^2)$ is independent of D_{app}.

Gelation mechanism of the at- and st-PVA solutions by inelastic light scattering

In addition to the analysis of the spinodal decomposition by elastic light scattering, it is of interest to consider that the diffusion coefficient for gels with a single phase assuring an equilibrium state reflects the fluctuation of refractive index associated with thermal fluctuation of cross-linking joints. Thus, Tanaka and co-workers[32,33] determined the elastic modulus of polyacrylamide gels as a function of temperature from the measurements of magnitude of scattered intensity and also determined the diffusion coefficients of the gel from the characteristic time of concentration fluctuation of the polymer network. They pointed out that the diffusion coefficient is related to the ratio of the appropriate elastic modulus and a friction coefficient, based on the solution of linear equations associated with the second law of Newton.

Apart from their estimations[32,33], inelastic light scattering measurements were applied to PVA gels to obtain the diffusion coefficient in a typical simple system assuming the second law of Fick. In such a complicated system as PVA gels, the same treatment as used by Tanaka and co-workers[32,33] is impossible, since the random motions in PVA gels cannot be assumed. The measurements were carried out to obtain the diffusion coefficient of PVA gels in the process of very slow phase separation. Here, we must emphasize the assumption that the equilibrium state in solution is maintained during the photon counting period of 5–15 min and the system is uniform in spite of the existence of anisotropic rods. Without this assumption, we cannot pursue the following discussion. The evaluation of the data was done by the histogram and cumulative methods for determining the distribution of decay rate of Γ from the observed correlation function[34–37].

The left-hand columns in *Figure 12* show an example of the auto-correlation function $A(\tau)$ at 45°C plotted against decay time for a 1% st-PVA solution with 70/30 composition, and the right-hand columns show the corresponding diffusion coefficients. The indicated times, 515 and 1026 min, are from the point when the sample was set at 45°C. The sample was prepared in the same way as that used for the measurements of $\ln(I)$ *versus* t by elastic light scattering. The solid curves in the left-hand columns are also auto-correlation functions recalculated from the histogram, and the calculations were carried out by assuming a unimodal system. The recalculated curves are in good agreement with the experimental results. The adoption of a unimodal system was decided on the basis of a preliminary finding that, although a bimodal-like or a trimodal-like distribution

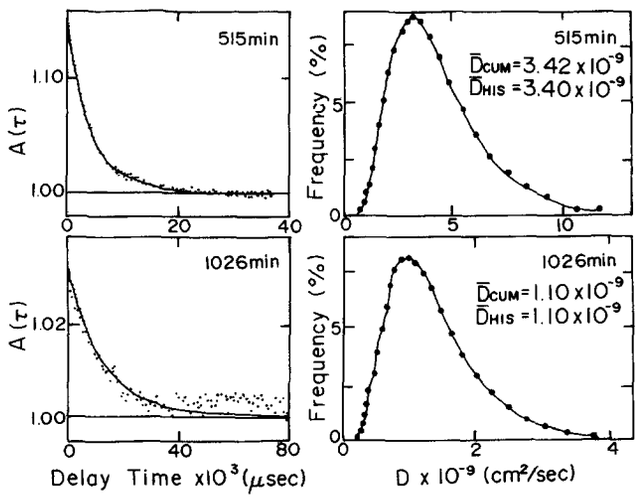

Figure 12 Left-hand columns: auto-correlation function $A(\tau)$ against delay time at 515 and 1026 min for the 1% solutions of 70/30 composition measured at 45°C. Plots are the experimental results and curves were recalculated from the histogram obtained assuring a unimodal system. Right-hand columns: distribution of diffusion coefficient D calculated by the histogram method. The curve was drawn to follow the points calculated for the centre of gravity of the distribution of the diffusion coefficient

gave a complicated histogram with one or two small peaks in addition to the main peak for the distribution of decay rate Γ, the auto-correlation functions recalculated from the complicated histogram were almost equal to those in *Figure 12*. Incidentally, analysis according to a bimodal-like or trimodal-like distribution is thought to be meaningless because of the broad molecular weight distribution of the present st-PVA with $M_w/M_n = 3.1$ and the at-PVA with 3.5. To estimate the diffusion coefficient, it is important to check that the plots yield a linear relationship, thus assuring the definition of $\bar{D}$ by $\Gamma = \bar{D}q^2$. The linear relationship was confirmed at time >6 h. As shown in the lower columns, the mean values ($\overline{D_{HIS}}$) estimated as the centre of gravity of the distribution curve are in good agreement with those of $\overline{D_{CUM}}$ calculated by the cumulative method. In the time scale <6 h, however, the phase separation was too rapid to measure Γ at various values of q^2 assuming that the equilibrium state of PVA solution was maintained during the measurement at various θ values. This is due to the difficulty in checking the linear relationship of Γ against q^2 in the time scale <6 h.

Here, it should be noted that the diffusion coefficient at 1026 min is lower than that at 515 min. This implies further immobilization of st-PVA chains owing to the progression of gelation/crystallization with time. The same tendency was also observed for at-PVA. This means that the gels become stiffer with time.

Viscosity of the at- and st-PVA solutions

Figures 13 and *14* show specific viscosity η_{sp} plotted against temperature for the st- and at-PVA solutions, respectively, with 50/50 and 70/30 compositions at the indicated concentrations. Measurements were carried out after 15 min when the polymer/solvent mixture was well blended at 105°C for 40 min in an Ubbelohde type of capillary viscometer which had been set at the measuring temperature. The indicated temperatures >60°C were chosen to avoid rapid gelation during the measurements. Actually, at the indicated concentrations, the gelation temperature in an Ubbelohde type of capillary viscometer was a little bit lower than that defined in the Experimental section. This is evident in comparison with the phase diagrams shown in *Figures 6* and *7*. In *Figure 13*, it is seen that for the 1% st-PVA solution, the value of η_{sp} for the 70/30 composition is higher than that for the 50/50 one in the given temperature range. At other concentrations, the values for the 50/50 composition

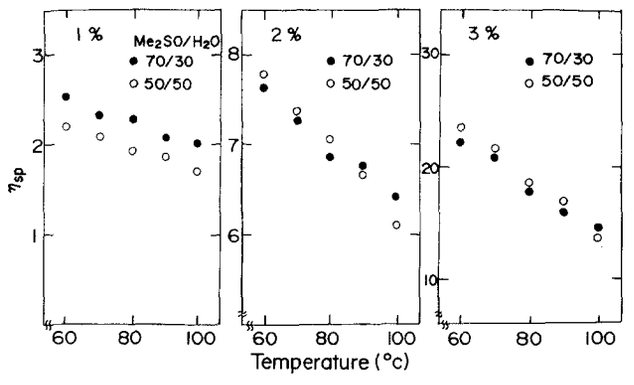

Figure 13 Specific viscosity η_{sp} against temperatures measured for the 1, 2 and 3% st-PVA solutions of 50/50 and 70/30 compositions

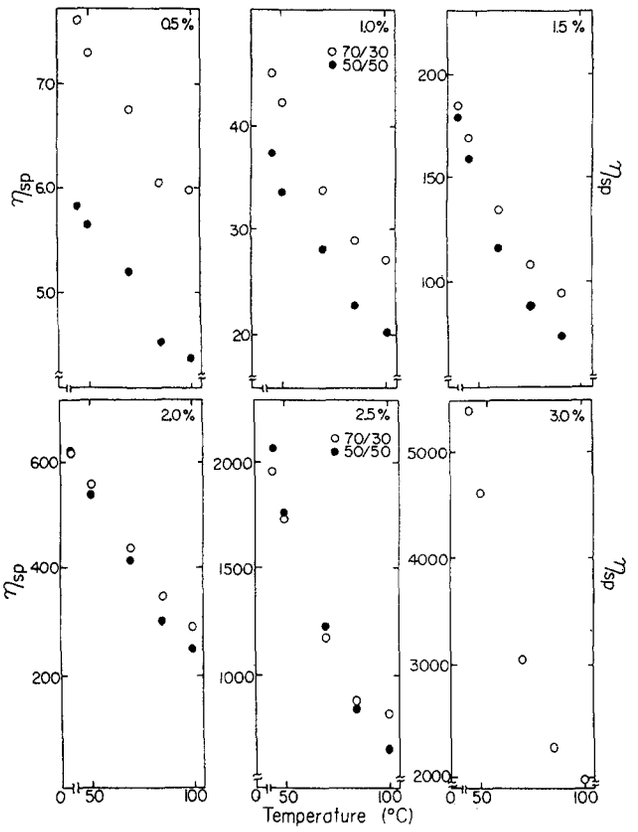

Figure 14 Specific viscosity η_{sp} against temperatures measured for the 0.5, 1 and 1.5% at-PVA solutions of 50/50 and 70/30 compositions

are also the same as those for the 70/30 one within experimental error. At the 1% concentration, the mixed solvent with 70/30 composition is thought to be a good solvent for st-PVA chains in comparison with that of the 50/50 composition, if viscosity depends on the radius of gyration and the overlap concentration of chains. Judging from the experimental results in *Figures 6* and *10*, the gelation mechanism by quenching the 1% solutions is in contradiction with the reported concept that the frequency of contact of the mean radius of gyration of st-PVA chains plays an important role in the gelation[38]. The contradiction suggests the fact that gelation of st-PVA solution as discussed before is not due to formation of a homogeneous infinite network from interpenetrating coils, but to phase separation of the solutions owing to thermodynamical instability.

The same phenomenon was also observed for at-PVA with $P = 17\,900$, as shown in *Figure 14*. The value for the 70/30 composition was higher than that for the 50/50 one at concentrations <1.5%, but the difference became less pronounced with increasing concentration and finally the values became almost the same at concentrations >2.5%. However, the gelation for the solutions with 50/50 composition occurred rapidly in comparison with those with 70/30 composition, when at-PVA solutions with concentrations <2% were quenched at the same temperature. This result also supports the gelation of at-PVA solutions due to retarded phase separation. Here, it should be noted that significant drawability of the resulting film is affected by the characteristics of PVA chains in dilute solutions. Namely, the frequency of contact of the mean radius of the 1% PVA solution causes a significant effect on drawability, since the

maximum draw ratio at the 70/30 composition is higher than that at the 50/50 one (see *Figure 1*).

Morphology and mechanical properties of the at- and st-PVA films with the greatest drawability

Through the experiments in *Figures 1–14*, it is evident that one of the important factors for determining the morphology and mechanical properties of the resulting films can be traced to the characteristics of the phase separation of st- and at-PVA solutions. To derive the conclusive evidence, the deformation mechanism and mechanical properties were estimated for at- and st-PVA films drawn up to their maximum draw ratios, in detail. Due to the preliminary experimental results assuring the greatest significant drawability in *Figure 1*, the films were prepared by quenching at-PVA solutions at −80°C and vacuum-drying at room temperature. The contents of Me_2SO as co-solvent were set at 60 and 70 vol%. Before evaporating the solvent, the resulting gels were stored for one day at −80°C. The two-stage elongations of films were performed by using the method described in the Experimental section.

The left- and right-hand columns of *Figure 15* show crystallinity as a function of draw ratio of λ for at-PVA and st-PVA films, respectively, prepared from the solutions with 60/40 and 70/30 compositions. The crystallinity for the at-PVA films shows a gradual increase with λ and attains a value of 40% beyond $\lambda = 12$. This tendency is almost independent of the composition. The change in crystallinity of the st-PVA film shows almost the same tendency, but the value reaches about 50% beyond $\lambda = 12$, indicating that the alignment of st-PVA chains with high stereo-regularity promotes an increase in crystallinity. The value for st-PVA films at each draw ratio are higher than those for the at-PVA films. Even so, the maximum value is much lower than that reported for ultradrawn polyethylene[39]. This is one of the factors to disturb the drastic improvement of the Young's modulus of the drawn PVA films, as will be discussed later.

To study the molecular orientation of the at- and st-PVA films, the second-order orientation factor, F_{200}^b, of the *b*-axis (the crystal chain axes) was obtained and the results are shown in *Figure 16*. F_{200}^b characterizes the orientation distribution of the *b*-axes with variation between −1/2 and 1. For random orientation, F_{200}^b is 0, while for complete orientation, parallel and perpendicular to the stretching direction, it is unity and −1/2, respectively. The orientation factor was estimated

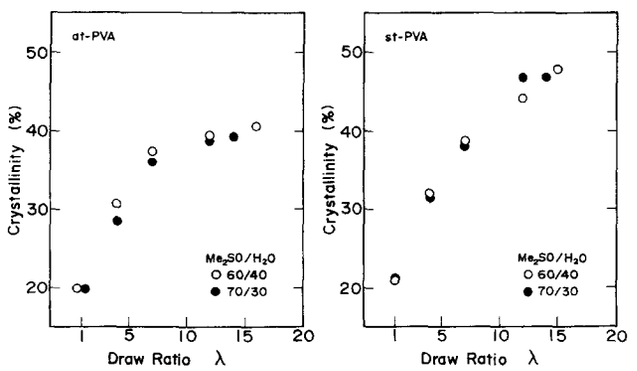

Figure 15 Change in crystallinity as a function of draw ratio λ for the at- and st-PVA films, prepared from the solutions with 60/40 and 70/30 compositions

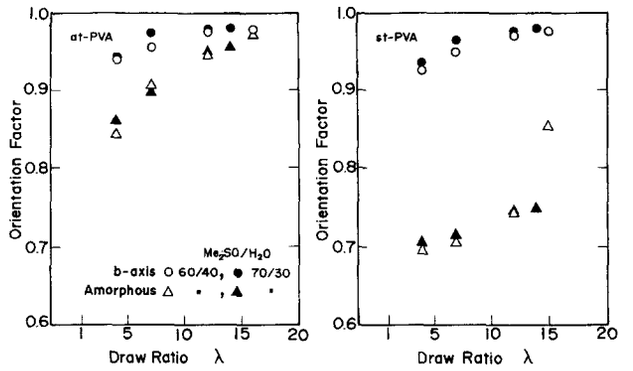

Figure 16 Change in the second-order orientation factor of the *b*-axis as a function of draw ratio of λ for the at- and st-PVA films, prepared from the solutions with 60/40 and 70/30 compositions

directly from the orientation distribution function of the (020) plane. At $\lambda = 4$, the orientation factor for the at-PVA is somewhat higher than that for the st-PVA, but with increasing λ the values for both specimens attained 0.98, indicating an extremely high orientational degree of the *b*-axis.

The second-order orientation factor, F_{200}^{am}, of the amorphous chain segments was determined from birefringence data obtained by subtraction of the crystalline contribution from the total birefringence, assuming simple additivity and neglecting the form birefringence as indicated in the following equation[40]:

$$\Delta_{total} = X_c\Delta_c + (1 - X_c)\Delta_a \quad (6)$$

where Δ_{total} is the total birefringence of the bulk specimen, and X_c is the volume crystallinity. Δ_c is the crystalline birefringence, and Δ_a is the amorphous birefringence. In equation (6), Δ_c and Δ_a are given by

$$\Delta_c = \Delta_c^o F_{200}^b \quad (7)$$

and

$$\Delta_a = \Delta_a^o F_{200}^{am} \quad (8)$$

where Δ_c^o and Δ_a^o are the intrinsic birefringences of the crystal and amorphous phases, respectively. The procedure for evaluating the intrinsic birefringences of crystalline and amorphous phases is quite similar to that described earlier[41]. These values were estimated by utilizing the values of bond polarizabilities proposed by Bunn and Daubeny[42], the crystal structure by Nitta *et al.*[43] and the values of crystalline and amorphous densities (1.345 and 1.269, respectively) by Sakurada *et al.*[44] to give the following values: $\Delta_c^o = 0.0443$ and $\Delta_a^o = 0.0404$[41].

The results are also shown in *Figure 16*. Before the measurements were made, X-ray diffraction patterns from both the specimens with $\lambda > 4$ were confirmed to be almost circular diffraction rings, indicating a uniaxial orientation of crystallites with respect to the stretching direction, when an incident beam was directed parallel to the stretching direction (end view). It is seen that F_{200}^{am} is lower than F_{200}^b at each draw ratio and this tendency is considerable at lower draw ratio $\lambda < 10$. This phenomenon can be analysed on the basis of the change in the *Hv* light scattering pattern under elongation. To explain this, we shall refer to the change in the *Hv* patterns briefly, although the patterns are not shown in this paper. In spite of clear X-type patterns from the at- and st-PVA

gels, the scattering from the film after the evaporation of solvent displays indistinct circular patterns in which the intensity decreases continuously with increasing scattering angle, but does not vary with the azimuthal angle, indicating a typical scattering from a system composed of a random array of crystallites that are smaller compared with the wavelength of the incident beam. For the present at- and st-PVA films, elongation beyond $\lambda = 4$ causes development of a clear X-type pattern whose lobes are extended in the meridional direction. Such a similar pattern was also observed for the at-PVA ($P = 2000$) as reported already in the previous paper[5]. Furthermore, a small angle X-ray pattern showed a scattering maximum in the film thickness direction, indicating the existence of folded crystal lamellae. To explain such unusual uniaxial orientational behaviour of rods, one model was proposed in the previous paper[5], in which a scattering unit corresponds to a new rod-like structure that is formed by a lateral coalescence of rods during elongation. The model system allows one to imagine that the new structure is mainly composed of crystallites whose chain axes are oriented in the stretching direction and that the amorphous chain segments play an important role in connecting two neighbouring new structures as entanglements and/or tie molecules. Accordingly, the orientational degree of the amorphous chain segments becomes automatically lower than that of the *b*-axes, and the orientational degree of the amorphous chain segments for the st-PVA ($P = 1980$) becomes lower than that for the at-PVA ($P = 17900$), although the *b*-axes for the at- and st-PVA films take the same orientational degree. This concept can be explained in terms of the chain length of the amorphous segments. Namely, the extended chain length of the st-PVA is thought to be much shorter than that of the at-PVA, since most of the amorphous parts fill to perform entanglement meshes and/or tie molecules.

Figure 17 shows the change in Young's modulus as a function of draw ratio of λ for the at- and st-PVA films. The increase in Young's modulus with λ is more significant for the at-PVA films and the maximum value reached 43 GPa, while that for the st-PVA films reached 39 GPa. Considering the three results in *Figures 15–17*, it is obvious that the higher value for the at-PVA film is affected by the significant orientation of amorphous chain segments, since the orientational degree of the *b*-axis and the crystallinity for the both specimens are quite similar to each other. Anyway, the difference of the

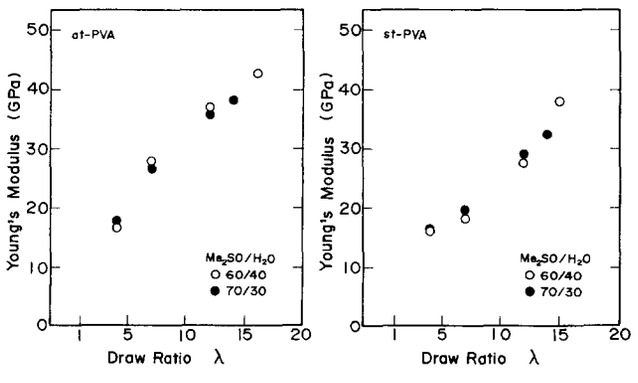

Figure 17 Change in Young's modulus as a function of draw ratio of λ for the at- and st-PVA films, prepared from the solutions with 60/40 and 70/30 compositions

Young's modulus between the at- and st-PVA films is not so significant. Here, it may be noted that, when the at-PVA films could be elongated by the two stages as described in the Experimental section, the maximum Young's modulus reached 43 GPa. This maximum value is higher than the value (34.7 GPa) of the at-PVA drawn at 160°C (see *Figure 1*). This indicates that the elongation temperature plays an important role in improving Young's modulus, accompanying the improvement of maximum draw ratio. Through the further experimental results, we confirmed that, by the elongation of specimens annealed at 220°C for several minutes, Young's modulus reached 80 GPa, close to the values reported by several authors[2–4]. However, the specimens browned, although the X-ray diffraction pattern was not changeable. Most of the PVA reports have never referred to the colour of the specimens. However, if the specimens prepared by these authors browned, a question can arise as to whether or not the brownish PVA specimen should be utilized as a commercial material. Anyway, Young's modulus of PVA is much lower than the crystal lattice modulus (210–240 GPa)[44,45] in spite of the fact that the PVA chains are fully aligned at maximum draw ratio. This is quite different from the results for polyethylene whose Young's modulus is close to the crystal lattice modulus[39]. This is attributed to two factors: the crystallinity is less than 50% and the preferential orientation of the *b*-axes is due to the rotation of crystallites independent of crystal transformation from a folded to a fibrous type[5].

As conclusive evidence, the greatest significant drawability of PVA films is clearly related to the phase separation of the solutions. As shown in *Figure 2*, the continuous texture with honeycomb-like structure is similar to the phase separation by spinodal decomposition as has been observed for amorphous blend polymers[23]. Thus, it may be expected that rapid phase separation of at-PVA solutions is due to the thermodynamic instability and subsequently gelation/crystallization occurs in the polymer-rich phase. Consequently, the greatest significant drawability can be realized by a continuous, uniform, fine fibrous texture with no optical anisotropy, since such a continuous structure can transmit inner stress smoothly under the elongation process. To check the validity of this concept, two kinds of gels were prepared from the 1% st- and at-PVA solutions with 70/30 composition according to the same method as employed for preparation of the specimens to measure $\ln(I)$ *versus* t in *Figures 8* and *9*. After 150 min, the two gels were quenched at −80°C to stop the further progression of phase separation. Thereafter, the co-solvent was evaporated from the resulting swollen gels. The elongation of dry films was carried out by the same method in *Figure 15*. The maximum draw ratios of the st- and at-PVA films were in the range 13–14 and Young's moduli were lower than those in *Figure 17*. The fibrous texture under SEM was similar to that of film prepared at −10°C in *Figure 2*. The hole size of the honeycomb-like structure was larger than that of the film prepared by rapidly quenching the at-PVA solutions at −80°C.

Through a series of experimental results, it may be expected that rapid phase separation of polymers probably occurs within the time scale of gel and wet spinning speeds. Actually, the continuous structure has been observed within mono-filaments of polyacrylonitrile by wet spinning and within polyethylene films by

gelation/crystallization from dilute solutions. It may be expected that such a structure plays an important role in carrying out gel and wet spinnings without scission of filaments.

CONCLUSIONS

Two main conclusions can be drawn:

(1) Phase separation of at-PVA ($P = 17900$) and st-PVA ($P = 1980$) was studied by light scattering techniques, using mixtures of dimethyl sulfoxide and water as a co-solvent. The logarithm of scattered intensity against time yielded a straight line, as has been confirmed in the initial stage of spinodal decomposition, and started to deviate from this linear relationship in the latter stage. In the later stage, however, an X-type pattern, indicating the existence of anisotropic rods, could be observed. The maximum growth rate $R(q_m)$ of concentration fluctuation increased with decreasing temperature. The value of the scattering vector, q_m, shifted slightly toward the scattering centre with increasing difference $(T_s - T)$ between the measurable temperature, T, and spinodal temperature T_s. These phenomena were quite different from the principle of spinodal decomposition of amorphous polymer solutions proposed by van Aartsen[19]. In particular, for the 1% st-PVA solution with 50/50 composition at 55°C, whose phase diagram corresponds to a sol region under spinodal temperature indicating only spinodal decomposition, an X-type pattern could be observed even in the initial stage, assuring linear plots of $\ln(I)$ *versus* t. Such a contradiction is thought to be due to the criterion defined for gelation: the meniscus deformed, but the specimen did not flow under its own weight when the solution in a test-tube was tilted. This indicates that, even in the region observed as a sol, gelation occurred locally within the sol region at the macroscopic level.

(2) The morphology and mechanical properties of the films prepared by quenching solutions and by evaporating solvents can be traced to the characteristics of the phase separation of st- and at-PVA solutions. When the solution was quenched at temperatures <-10°C and vacuum-dried, the resulting films maintained transparency. Under SEM, the tissue within the film showed honeycomb-like structure similar to continuous tissue characterizing spinodal decomposition of solutions due to thermodynamic instability. The hole size of the honeycomb-like structure became smaller as the quenching temperature decreased, but the size within each specimen prepared by quenching solutions at various temperature was almost constant. The hole size observed within films, which were prepared by quenching solutions at -80°C and drying, was within the limit of the characteristic wavelength of a polymer–solvent system. Even so, any scattering ring could not be observed for swollen gels and dry gel films under V_v polarization and depolarization conditions. The appearance of honeycomb-like structure indicated that gelation of PVA solutions was not due to formation of a homogeneous infinite network from interpenetrating coils, but due to the phase separation of solutions owing to thermodynamic instability. This indicates that further development of gelation/crystallization is pronounced by immobilization of PVA chains in the polymer-rich phase. The draw ratio increased as the quenching temperature decreased, when the dimethyl sulfoxide content was set in the range 60–70 vol%. The greatest significant drawability was realized by quenching solutions at -80°C, and the corresponding Young's modulus took a maximum value. Thus, it turns out that the dense network structure plays an important role in assuring significant drawability in order to transmit inner stress smoothly in the stretching direction.

REFERENCES

1. Cha, W. I., Hyon, S. H. and Ikada, Y., *J. Polym. Sci., Part B: Polym. Phys.*, 1994, **32**, 297.
2. Kunugi, T. and Kawasumi, T., *IUPAC 32nd International Symposium on Macromolecules Prepr.*, 1988, p. 431.
3. Yamaura, K., Itoh, H., Tanigami, T. and Matsuzawa, S., *J. Appl. Polym. Sci.*, 1987, **34**, 2347.
4. Yamaura, K., Tanigami, Y., Hayashi, N., Kosuda, K., Okuda, S., Takemura, Y., Itoh, M. and Matsuzawa, S., *J. Appl. Polym. Sci.*, 1990, **40**, 905.
5. Sawatari, C., Yamamoto, Y., Yanagida, N. and Matsuo, M., *Polymer*, 1993, **34**, 956.
6. Matsuo, M., Kawase, M., Sugiura, Y., Takematsu, S. and Hara, C., *Macromolecules*, 1993, **26**, 4461.
7. Nishinari, K., Watase, M., Ogino, K. and Nambu, M., *Polym. Commun.*, 1983, **24**, 345.
8. Watase, M. and Nishinari, K., *Makromol. Chem.*, 1988, **189**, 871.
9. Yamaura, K., Itoh, M., Tanigami, T. and Matsuzawa, S., *J. Appl. Polym. Sci.*, 1989, **37**, 2709.
10. Stauffer, S. R. and Peppas, N. A., *Polymer*, 1992, **33**, 3932.
11. Farrant, J., *Nature*, 1965, **205**, 1284.
12. Friedberg, F., Brown, W., Henley, D. and Ohman, J., *Makromol. Chem.*, 1983, **66**, 168.
13. Smith, P., Lemstra, P. J., Pippers, J. P. and Kiel, A. M., *Coll. Polym. Sci.*, 1981, **258**, 1070.
14. Matsuo, M. and Manley, R. S. T., *Macromolecules*, 1982, **15**, 895.
15. Matsuo, M. and Manley, R. S. T., *Macromolecules*, 1983, **16**, 1500.
16. Matsuo, M., Inoue, K. and Abumiya, N., *Sen-i-Gakkaishi*, 1984, **36**, 696.
17. Cahn, J. W., *J. Chem. Phys.*, 1965, **42**, 93.
18. Cahn, J. W. and Hilliard, J. E., *J. Chem. Phys.*, 1958, **28**, 258.
19. van Aartsen, J. J., *Eur. Polym. J.*, 1970, **6**, 919.
20. Hashimoto, T., Kumaki, J. and Kawai, H., *Macromolecules*, 1983, **16**, 641.
21. Nishi, T., Wang, T. T. and Kwei, T. K., *Macromolecules*, 1975, **8**, 227.
22. Rhodes, M. and Stein, R. S., *J. Polym. Sci., Part A-2*, 1969, **7**, 1539.
23. Sakurada, I., Nukushina, K. and Sone, Y., *Kobunshi Kagaku*, 1955, **12**, 506.
24. Komatsu, M., Inoue, T. and Miyasaka, K., *J. Polym. Sci.*, 1986, **24**, 303.
25. Langer, J. S., Bar-on, M. and Miller, H. S., *Phys. Rev. Lett.*, 1974, **11**, 1417.
26. Debye, P. and Woermann, D., *J. Chem. Phys.*, 1962, **36**, 1803.
27. Hung, J. S., Goldburg, M. I. and Bjer Kaas, A. M., *Phys. Rev. Lett.*, 1974, **32**, 921.
28. McMaster, L. P., *Adv. Chem. Ser (ACS)*, 1975, **142**, 43.
29. Labudzinska, A. and Ziabicki, A., *Kolloid Z.Z. Polym.*, 1971, **243**, 21.
30. Wellinghoff, S. W., Shaw, J. and Beat, E., *Macromolecules*, 1979, **12**, 932.
31. Kobayashi, M., Ando, I., Ishii, T. and Amiya, S., *Macromolecules*, 1995, **28**, 6677.
32. Tanaka, T., Hocker, L. O. and Benedek, G. B., *J. Chem. Phys.*, 1973, **59**, 5151.
33. Tanaka, T. and Fillmore, D. J., *J. Chem. Phys.*, 1979, **70**, 1214.
34. Berne, B. J. and Pecora, R., *Dynamic Light Scattering*. John Wiley, New York, 1976, pp. 85–126.

35. Chu, B., *Laser Light Scattering*. Academic Press, New York, 1974, pp. 53–90.
36. Koppel, D. E., *J. Chem. Phys.*, 1972, **57**, 4814.
37. Nemoto, N., Tsunashima, Y. and Kurata, M., *Polym. J.*, 1981, **13**, 827.
38. Ohkura, M., Kanaya, T. and Kaji, K., *Polymer*, 1992, **33**, 3686.
39. Matsuo, M. and Sawatari, C., *Macromolecules*, 1986, **19**, 2036.
40. Stein, R. S. and Norris, F. H., *J. Polym. Sci.*, 1956, **21**, 381.
41. Nomura, S. and Kawai, H., *J. Polym. Sci., Part A-2*, 1966, **4**, 797.
42. Bunn, C. W. and Daubeny, R. de P., *Trans. Faraday Soc.*, 1954, **50**, 1173.
43. Nitta, I., Taguchi, I. and Chatani, Y., *Ann. Rep. Inst. Fiber Sci., Osaka Univ.*, 1957, **10**, 1.
44. Sakurada, I., Nukushina, Y. and Ito, T., *J. Polym. Sci.*, 1962, **57**, 651.
45. Matsuo, M., Haarashina, Y. and Ogita, T., *Polymer J.*, 1993, **25**, 319.